Photoinduced Charge Carrier Dynamics and Electron Injection Efficiencies in Au Nanoparticle-Sensitized TiO_2 Determined with Picosecond Time-Resolved X-ray Photoelectron Spectroscopy

Mario Borgwardt[1], Johannes Mahl[1], Friedrich Roth[2], Lukas Wenthaus[3], Felix Braußе[1], Monika Blum[1,4], Klaus Schwarzburg[5], Guiji Liu[1,6], Francesca M. Toma[1,6], and Oliver Gessner[1]*

[1]Chemical Sciences Division, Lawrence Berkeley National Laboratory, Berkeley, California 94720, USA

[2]Institute of Experimental Physics, TU Bergakademie Freiberg, D-09599 Freiberg, Germany

[3]Deutsches Elektronen Synchrotron / DESY, D-22607 Hamburg, Germany

[4]Advanced Light Source, Lawrence Berkeley National Laboratory, Berkeley, California 94720, United States

[5]Institute for Solar Fuels, Helmholtz-Zentrum Berlin für Materialien und Energie GmbH, 14109, Berlin, Germany

[6]Joint Center for Artificial Photosynthesis, Lawrence Berkeley National Laboratory, California 94720, USA

*corresponding author: ogessner@lbl.gov

Abstract

Progress in the development of plasmon-enabled light-harvesting technologies requires a better understanding of their fundamental operating principles and current limitations. Here, we employ picosecond time-resolved X-ray photoemission spectroscopy to investigate photoinduced electron transfer in a plasmonic model system composed of 20 nm sized gold nanoparticles (NPs) attached to a nanoporous film of TiO_2. The measurement provides direct, quantitative access to transient local charge distributions from the perspectives of the electron donor (AuNP) and the electron acceptor (TiO_2). On average, approximately two electrons are injected per NP, corresponding to an electron injection yield per absorbed photon of 0.1%. Back electron transfer from the perspective of the electron donor is dominated by a fast recombination channel proceeding on a timescale of 60±10 ps and a minor contribution that is completed after ≈1 ns. The findings provide a detailed picture of photoinduced charge carrier generation in this NP-semiconductor junction, with important implications for understanding achievable overall photon-to-charge conversion efficiencies.

TOC GRAPHICS

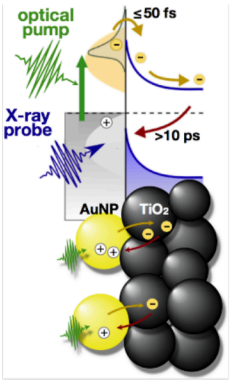

KEYWORDS: interfacial charge transfer, time-resolved X-ray photoelectron spectroscopy, plasmonic nanoparticles, photocatalysis, titanium dioxide

The conversion of solar energy into chemical fuels via photoelectrochemical (PEC) splitting of water into hydrogen and oxygen is an important component of strategies to achieve a carbon-neutral economy.[1] Heterogeneous systems consisting of plasmonic metal nanoparticles (NPs) attached to wide band gap semiconductor (SC) materials have been identified as a promising approach for renewable energy technologies based on PEC. The heterogeneous design enables increased light absorption, enhanced charge carrier separation and higher photocatalytic reactivity compared to bare wide band gap materials.[2]

The canonic model for plasmon-enabled charge generation processes at NP-SC interfaces is based on light absorption via localized surface plasmon resonances (LSPR), followed by ultrafast plasmon damping and dephasing, resulting in the population of hot electrons that are able to transfer to the SC conduction band (Fig. 1a).[3–5] Variations of this mechanism including, for example, plasmon-enabled interfacial charge-transfer excitations have been proposed as well.[6,7] Despite substantial efforts to develop plasmonic light-harvesting devices, overall device efficiencies remain quite low with most groups reporting external quantum efficiencies well below one percent[8–12] and only a few reaching higher values of a few percent.[13,14] The underlying physical limitations are not well understood and may include low charge injection efficiencies as well as challenges associated with light absorption, charge transport, back electron transfer or low yields of the catalytic reaction at the SC-liquid interface. Disentangling these individual restrictions remains challenging. In particular, the determination of NP-SC charge injection and back electron transfer rates requires time domain techniques that, ideally, are sensitive to short-lived, local charge densities. Time-resolved studies in the visible and infrared (IR) regimes monitor spatially averaged, free charge carrier densities in the SC acceptor,[3,15–17] and have led to photon-to-electron injection efficiency estimates of up to 50%.[6,15,17,18] Theoretical predictions,

however, vary only between a few[6] and up to 20%[19], and the root causes for the discrepancies between theory and experiment have yet to be identified. New techniques are sought that can provide a direct, quantitative measure of the time-dependent amount of charge inside the plasmonic NPs as well as the transient charge- and energy-distributions within the immediate, nanometer scale interfacial region between and the NPs and the SC.[20]

Here, we apply picosecond time-resolved X-ray photoelectron spectroscopy (TRXPS) to gain a site-specific perspective on photoinduced charge-transfer dynamics at the interface between spherical gold NPs (20 nm diameter) and a nanoporous TiO_2 substrate. The results provide an absolute measure of the amount of charge injected from the AuNPs into the SC substrate, indicating that ~2 electrons are transferred per NP, corresponding to a photon-to-charge conversion efficiency of ~0.1 %. Electron-hole recombination is completed within ~1 ns. The study provides the first reference-free, quantitative, microscopic, real-time insight into the efficiency and temporal evolution of charge transfer dynamics in a standard nanoplasmonic heterostructure. It demonstrates that currently available benchmark values for the first steps of photon-to-charge conversion in AuNP-sensitized TiO_2 need to be re-evaluated based on newly available data and corresponding theoretical estimates. The observations also bear consequences for the design of more efficient nanoplasmonic solar light harvesting devices as discussed below.

In the TRXPS experiment, interfacial charge-transfer dynamics are initiated by 10 ps long optical (532 nm) pump pulses and probed site-specifically at both the electron donor (AuNP) and acceptor (TiO_2) by transient changes in the Au4f and Ti2p photolines, respectively. The measurements are performed at Beamline 11.0.2 of the Advanced Light Source (ALS), using 70 ps long X-ray pulses with photon energies of $h\nu$=687 eV for the Au4f and $h\nu$=950 eV for the

Ti2p lines (see Supporting Information for further details on sample preparation and the TRXPS experiment).

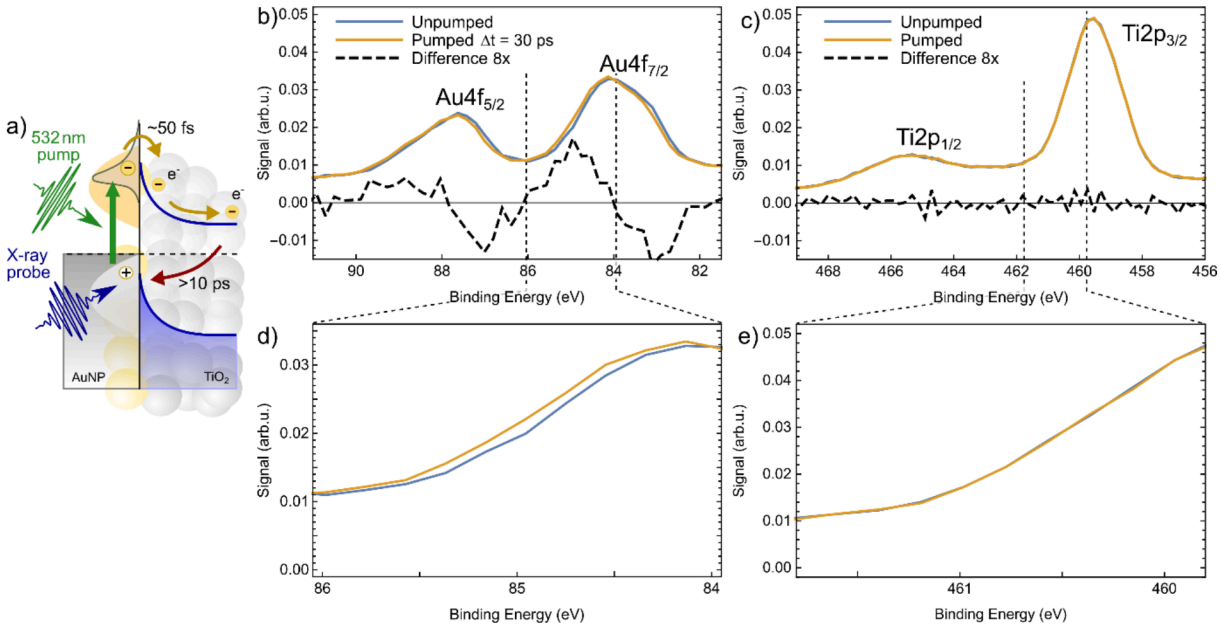

Figure 1. a) Illustration of the optical pump / X-ray-probe experiment with relevant processes and timescales at the AuNP – TiO_2 interface. (b,c) TRXPS spectra of AuNP sensitized, nanoporous films of TiO_2: Comparison of the Au4f (b) and Ti2p (c) photolines before optical excitation (blue) and at a pump-probe delay of Δt=30 ps (orange). The dashed black lines indicate the differences between the excited and ground state spectra, multiplied by a factor of 8 for better visibility. Panels d) and e) show magnified views of selected spectral ranges as indicated.

Figure 1b,c shows TRXPS spectra of the Au4f (b) and Ti2p (c) signals before laser excitation (blue) and at a pump-probe delay of Δt=30 ps (orange) for a pump-laser fluence of 0.2 mJ/cm^2. The Au4f spectrum consists of the $Au4f_{5/2}$ and $Au4f_{7/2}$ peaks at 87.7 eV and 84.0 eV binding energy, respectively.[21] The Ti2p spectrum is composed of the Ti $2p_{1/2}$ and Ti $2p_{3/2}$ spin-orbit components with binding energies of 465.3 and 459.4 eV, respectively.[22] The black dashed curves correspond to the differences between the excited and the ground state spectra, multiplied by a factor of 8 for better visibility. No spectral change is observed in the Ti2p spectrum upon pump laser interaction within the signal-to-noise of the measurement. In contrast, the Au4f

spectrum exhibits a distinct response to laser excitation, leading to a bipolar structure in the difference curve for each spin-orbit component. To achieve a large acceptance solid angle for photoelectrons, an electrostatic lens system is used that leads to peak broadening but does not affect the measured shifts. The laser-induced XPS response is modeled by a rigid shift of the entire spectrum to higher binding energies. The extent of this shift is determined to ~80 meV by minimizing the difference between the neutral ground state spectrum and a shifted version of the spectrum recorded after laser excitation. In order to exclude any effects arising solely from the AuNPs, additional reference measurements are conducted that monitor the Au4f and Al2p TRXPS spectra of AuNPs deposited on Al_2O_3 substrates. In this configuration, Al_2O_3 inhibits charge transfer at the NP-SC interface, enabling the investigation of the isolated AuNP response. No photoresponse is detected in either the Au4f or the Al2p photolines of the AuNP-Al_2O_3 control samples, confirming that the transient Au4f photoresponse of the AuNP-TiO_2 samples arises from electron injection from the AuNPs into the TiO_2 substrate (see Supporting Information for details).

Time-dependent shifts of the Au4f and Ti2p spectra as a function of pump-probe delay are derived using the spectral difference minimization procedure described above, leading to the red and green markers, respectively, in Fig. 2. The laser pulse precedes the X-ray pulse for positive delays. Positive energy shifts indicate spectra with higher binding energies after laser exposure compared to the neutral ground state spectra before the pump pulse arrives.

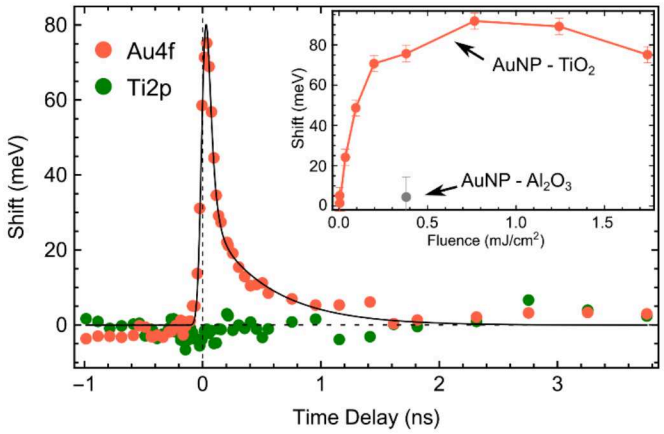

Figure 2. Site-specific, time-dependent photoresponse of the AuNP – TiO_2 interface at a pump laser fluence of 0.2 mJ/cm^2. Positive shifts correspond to higher binding energies after laser excitation compared to the ground state spectra. The Au4f photoresponse is described by a bi-exponential fit model convoluted with the IRF (solid line). The fit indicates an initial decay within τ_1=60±10 ps followed by slower signal fading on a timescale of τ_2=0.8±0.2 ns. The inset shows the fluence-dependence of the maximum Au4f photoresponse at Δt=30 ps for the TiO_2 substrate (red) and the Al_2O_3 reference substrate (gray).

While the Ti2p peak is essentially unaffected by the optical excitation across all time delays, the Au4f line exhibits a pronounced response that is maximal at ~30 ps delay and subsequently decays with the involvement of multiple timescales. The trend is modeled using the following bi-exponential fit function that includes a convolution with the instrument response function (IRF):

$$\Delta BE(t) = \left(A_1 \cdot e^{-t/\tau_1} + A_2 \cdot e^{-t/\tau_2}\right) * IRF \qquad (1)$$

The amplitudes A_1 and A_2 as well as the decay constants τ_1 and τ_2 are free fit parameters, while the IRF and time zero of the time-delay axis are fixed to the results of the IRF calibration measurements (see SI). The best fit, shown as a solid curve in Fig. 2, is in good agreement with the data and indicates that the response initially decays within τ_1=60±10 ps and vanishes on a characteristic timescale of τ_2=0.8±0.2 ns. Within this description, the actual maximum amplitude of the response is given by $A_1 + A_2$ = 200±30 meV (A_1=160±30 meV, A_2=40±10 meV). In the measurement, this amplitude is reduced to ~80 meV by the IRF.

The observed amplitude of the Au4f photoresponse at 30 ps delay is further investigated as a function of pump pulse fluence as illustrated in the inset of Fig. 2. The measurement reveals a nearly linear correlation between line shift and excitation fluence up to ≈0.2 mJ/cm^2, beyond which the observed response saturates at approximately 80 meV. In comparison, the control experiment on AuNP - Al_2O_3 (gray dot) at a fluence of about 0.4 mJ/cm^2 does not indicate any measurable photoresponse.

Plasmon-induced hot-electron transfer (HET) is the most prominently discussed charge transfer mechanism for nanoplasmonic light harvesting systems. It is based on the excitation and subsequent decoherence of a surface plasmon resonance, resulting in a population of hot electrons that are able to undergo ultrafast transfer to the SC (Fig. 1a). A direct, unambiguous proof for this picture is still outstanding. Being able to quantify the amount of charge that may be extracted after absorption of *n* photons in a plasmonic light absorber is essential in order to test this and alternative physical pictures. The observed transient photoresponse presented here gives direct, quantitative insight into the electron injection efficiency per NP and the subsequent electron-hole recombination dynamics as discussed in the following.

Electron transfer from the AuNP into TiO_2 will effectively lead to a positively charged metal sphere with the excess positive charge mainly residing at the NP surface. Within this picture, the missing charge creates an additional constant potential throughout the NP, leading to an increase in the effective binding energies of the Au4f core levels, as observed in the experiment. A theoretical model is needed to translate the measured core level shifts into the amount of NP valence charges created by the NP-SC charge transfer. A first-principles based, quantitative prediction of the AuNP core binding energies as a function of the number of transferred charges is rather challenging. Instead, we use a semiclassical jellium model to estimate the valence charge distribution within

the spherical metal clusters and its impact on the Au4f photoelectron kinetic energies.[23] Within the jellium model, the positive ion cores are represented by a uniform positive background charge density in the calculations.[24,25] The model predicts that excess or missing charge is accumulated within a surface layer with a width given by the Wigner-Seitz radius (R_{Wigner} = 0.165 nm for Au[26]), whereas the electron density inside the sphere stays largely unaffected. Fig. 3a schematically illustrates the electron density change for a positively charged sphere (blue solid line). The missing charge Q at the surface of the sphere with radius R_{sp}=10 nm creates a constant potential $V_Q = - Q/(4\pi\varepsilon_0 R_{sp})$ for all electrons inside the sphere and, thus, shifts their effective binding energies accordingly. Outside the sphere, the Coulomb potential decreases with 1/r, with r being the distance to the center of the sphere. The magnitude of the Coulomb potential can be considered constant throughout the XPS probing volume (see Fig. 3a, green line), which greatly simplifies the estimate of the induced shifts. The model predicts a linear dependence between observed binding energy shifts and the number of electrons injected into the SC. This is illustrated in Fig. 3b, which shows the predicted XPS peak shifts as a function of elementary charges removed from spherical AuNPs with various radii R_{SP} as indicated.

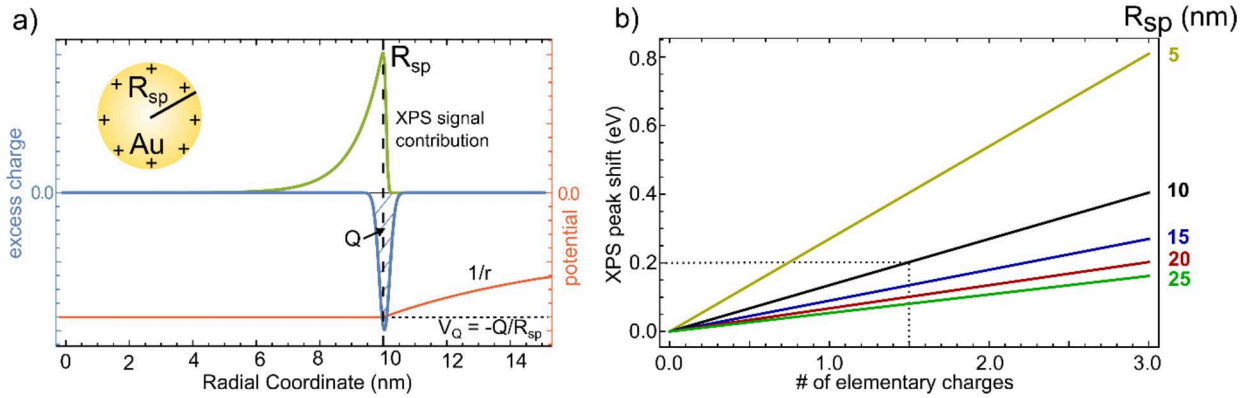

Figure 3. (a) Schematic of the electron density change (blue, left axis) induced by charge transfer from the AuNP into TiO_2 and the resulting effective potential (red, right axis) as a function of the radial coordinate measured from the center of the AuNP with a radius of R_{SP}=10 nm. The green curve represents relative XPS signal contributions based on the electron mean free path in gold. (b) Calculated XPS peak shifts as a function of the number of elementary charges on AuNPs with different radii R_{SP} as indicated. The dotted gray lines indicate the reconstructed maximum peak shift from the TRXPS measurement and the corresponding charge on the NPs used in this experiment.

Within this semiclassical approach, the reconstructed 200 meV Au4f binding energy shift obtained at a pump fluence of 0.2 mJ/cm^2 corresponds to injection of approximately 2 electrons per NP, assuming that all NPs within the probe volume contribute equally to the signal (gray dotted lines in Fig. 3b). This assumption is supported by the saturation of the photoresponse beyond 0.2 mJ/cm^2 as illustrated in the inset of Fig. 2. We note that the noise level of the measurement is on the order of ~5 meV. Requiring a measurable signal to be at least twice as large (~10 meV), this translates into a sensitivity of 1 electron leaving a AuNP with 300 nm diameter containing ~10^9 atoms.

The saturation fluence of 0.2 mJ/cm^2 corresponds to the absorption of approximately 2000 photons per AuNP based on their extinction coefficient of 9.2x10^8 $M^{-1}cm^{-1}$.[27] Correspondingly, the electron injection efficiency for this particular system, i.e., the number of injected electrons per absorbed photons, is on the order of 0.1%. This injection yield is significantly lower than those reported in several previous experimental investigations on hot charge carrier transfer in comparable systems. Estimates based on time-resolved optical absorption measurements range

from several hundred to several thousand electrons per NP of about half the size used here.[15,17,18] The substantial orders of magnitudes difference between the findings requires some attention. In particular, for time-resolved experiments utilizing short laser pulses / high peak fluences, the Coulomb potentials of the charged NP set boundaries to the maximum achievable injection efficiency both in terms of the energy that is required to overcome them as well as the maximum positive charge that may be supported by a NP without disintegration. The charge per NP measured here lies well within these energy and damage boundaries. A more detailed discussion of these aspects is provided in the Supporting Information. The measurement reveals a nearly linear correlation between line shift and excitation fluence up to ~0.2 mJ/cm^2, beyond which the observed response saturates at approximately 80 meV. A more detailed discussion of this trend is also provided in the SI.

The recovery of the Au4f ground state spectrum with a bi-exponential trend involving a fast 60±10 ps component and a slower 0.8±0.2 ns component reflects the back-electron transfer dynamics between the TiO_2 substrate and the AuNPs. The fast decay timescale observed here is in agreement with the findings of previous infrared (IR) transient absorption studies, which reported 1/e signal decays within ~20-100 ps.[15,18] It was shown that the TiO_2 particle size and sample preparation methods play an important role with regard to the overall lifetime.[18] Much faster initial signal decay within only 2ps was found for AuNPs fully embedded in ALD prepared TiO_2 films.[17] The observation of a significantly smaller charge carrier lifetime may arise from the different sample morphologies and/or could also be related to the different delay ranges and temporal resolution of the experiments.

The dominant sub-ns recombination timescales reported here and elsewhere may indicate a fundamental issue of the AuNP-TiO_2 system with respect to the achievable external photon-to-

current quantum yields. The electron diffusion coefficient D of TiO_2 films lies in a range of ~10^{-8} cm^2/s to ~10^{-5} cm^2/s.[28,29] Using the upper limit of D and a maximum lifetime of ~1 ns, the corresponding maximum diffusion length $L = \sqrt{D\tau}$ can be estimated to be on the order of ~1 nm. This is orders of magnitude smaller than, for example, diffusion lengths in dye-sensitized TiO_2 systems,[30,31] and indicates that efficient external charge extraction from a NP-TiO_2 heterojunction requires extremely thin SC domains.

Photoinduced charge transfer at the AuNP-TiO_2 interface results either in the generation of mobile charge carriers in the SC conduction band or the filling of trap states at the SC surface. Thus, transient spectral signatures with trends similar to those of the Au4f lines may also be expected in the Ti2p photolines. However, as can be seen in Fig. 1c, the ground and excited state spectra are indistinguishable within the experimental signal to noise ratio. Note that the missing Ti2p photoresponse cannot be associated with a lack of interfacial charge transfer in the AuNP-Ti2p system. The control experiment with the AuNP - Al_2O_3 sample confirms that the response of the Au4f lines in the AuNP – TiO_2 sample is due to photo-induced electron transfer. Therefore, the striking differences between the trends in the Au4f and Ti2p signals must be rooted in the different impacts of transient carrier densities in the donor and acceptor materials on their respective TRXPS signals. As discussed in more detail in the Supporting Information, we tentatively assign the missing Ti2p photoresponse to ultrafast surface-to-bulk diffusion of injected charges. Small total charge yields as well as the fact that the injected electron diffusion length is small compared to the AuNP size, leading to a "shadowing" effect that shields the injected electrons from detection, may also contribute.

The study illustrates the power of time-resolved X-ray photoelectron spectroscopy to investigate photoinduced charge transfer dynamics at interfaces between plasmonic NPs and nanoporous SC

substrates. The element-specificity of TRXPS allows to monitor transient, local charge distributions selectively from the perspectives of the electron donor (AuNP), complementing previous time resolved studies in the visible to IR regime. The transient increase of the effective Au4f binding energies provides a quantitative measure of the interfacial charge injection efficiency as well as the electron back transfer rate with a sensitivity of approximately one charge per 10^9 atoms. The observed photon-to-charge conversion efficiency of ~0.1% is significantly lower than values reported in some other studies but well within upper bounds set by theoretical predictions, fundamental energy conservation considerations, and target damage limits. The observed injection and electron-hole recombination dynamics provide important benchmarks for the design of plasmonic light harvesting systems. Future campaigns will investigate how the performance of the NP-SC interfaces correlates with parameters such as NP and SC materials and morphologies. Ultimately, the high sensitivity of TRXPS to transient local charges on a single electron level may enable the site-specific real-time monitoring of photoinduced chemical transformations enabled by heterogeneous nanoplasmonic assemblies.

Supporting Information. Sample preparation, Time-resolved XPS experiment and reproducibility, UV-VIS absorption spectra, Scanning electron microscopy (SEM), Control experiment with Al_2O_3 substrate, Rayleigh stability limit and total static potential energy, Fluence dependence of Au4f line shift, Photoresponse at the Ti2p edge
This material is available free of charge via the Internet

AUTHOR INFORMATION

corresponding author: ogessner@lbl.gov

Notes

The authors declare no competing financial interests.

ACKNOWLEDGMENT

This work was supported by the U.S. Department of Energy, Office of Science, Office of Basic Energy Sciences, Chemical Sciences, Geosciences and Biosciences Division, through Contract No. DE-AC02-05CH11231. This research used resources of the Advanced Light Source, a DOE Office of Science User Facility under contract no. DE-AC02-05CH11231. M.B. acknowledges support by the Alexander von Humboldt foundation. G.L. and F.M.T. are supported by the Joint Center for Artificial Photosynthesis, a DOE Energy Innovation Hub, supported through the Office of Science of the U.S. Department of Energy under Award Number DE-SC0004993.

REFERENCES

(1) Walter, M. G.; Warren, E. L.; McKone, J. R.; Boettcher, S. W.; Mi, Q.; Santori, E. A.; Lewis, N. S. Solar Water Splitting Cells. *Chem. Rev.* **2010**, *110*, 6446–6473, DOI:10.1021/cr1002326.

(2) Linic, S.; Christopher, P.; Ingram, D. B. Plasmonic-Metal Nanostructures for Efficient Conversion of Solar to Chemical Energy. *Nat. Mater.* **2011**, *10*, 911–921, DOI:10.1038/nmat3151.

(3) Cushing, S. K.; Li, J.; Meng, F.; Senty, T. R.; Suri, S.; Zhi, M.; Li, M.; Bristow, A. D.; Wu, N. Photocatalytic Activity Enhanced by Plasmonic Resonant Energy Transfer from Metal to Semiconductor. *J. Am. Chem. Soc.* **2012**, *134*, 15033–15041, DOI:doi.org/10.1021/ja305603t.

(4) Zhang, X.; Chen, Y. L.; Liu, R.-S.; Tsai, D. P. Plasmonic Photocatalysis. *Rep. Prog. Phys.* **2013**, *76* , 046401, DOI:doi.org/10.1088/0034-4885/76/4/046401.

(5) Christopher, P.; Moskovits, M. Hot Charge Carrier Transmission from Plasmonic Nanostructures. *Annu. Rev. Phys. Chem.* **2017**, *68*, 379–398, DOI:10.1146/annurev-physchem-052516-044948.

(6) Wu, K.; Chen, J.; McBride, J. R.; Lian, T. Efficient Hot-Electron Transfer by a Plasmon-Induced Interfacial Charge-Transfer Transition. *Science* **2015**, *349*, 632–635, DOI:doi.org/10.1126/science.aac5443.

(7) Li, J.; Cushing, S. K.; Meng, F.; Senty, T. R.; Bristow, A. D.; Wu, N. Plasmon-Induced Resonance Energy Transfer for Solar Energy Conversion. *Nat. Photonics* **2015**, *9*, 601–607, DOI:doi.org/10.1038/nphoton.2015.142.

(8) Mubeen, S.; Lee, J.; Singh, N.; Krämer, S.; Stucky, G. D.; Moskovits, M. An Autonomous Photosynthetic Device in Which All Charge Carriers Derive from Surface Plasmons. *Nat. Nanotechnol.* **2013**, *8*, 247–251, DOI:10.1038/nnano.2013.18.

(9) DeSario, P. A.; Pietron, J. J.; DeVantier, D. E.; Brintlinger, T. H.; Stroud, R. M.; Rolison, D. R. Plasmonic Enhancement of Visible-Light Water Splitting with Au–TiO2 Composite Aerogels. *Nanoscale* **2013**, *5*, 8073–8083, DOI:10.1039/C3NR01429K.

(10) Bian, Z.; Tachikawa, T.; Zhang, P.; Fujitsuka, M.; Majima, T. Au/TiO2 Superstructure-Based Plasmonic Photocatalysts Exhibiting Efficient Charge Separation and Unprecedented Activity. *J. Am. Chem. Soc.* **2014**, *136*, 458–465, DOI:10.1021/ja410994f.

(11) Ng, C.; Cadusch, J. J.; Dligatch, S.; Roberts, A.; Davis, T. J.; Mulvaney, P.; Gómez, D. E. Hot Carrier Extraction with Plasmonic Broadband Absorbers. *ACS Nano* **2016**, *10*, 4704–4711, DOI:10.1021/acsnano.6b01108.

(12) Ahn, W.; Ratchford, D. C.; Pehrsson, P. E.; Simpkins, B. S. Surface Plasmon Polariton-Induced Hot Carrier Generation for Photocatalysis. *Nanoscale* **2017**, *9*, 3010–3022, DOI:10.1039/C6NR09280B.

(13) Tian, Y.; Tatsuma, T. Mechanisms and Applications of Plasmon-Induced Charge Separation at TiO2 Films Loaded with Gold Nanoparticles. *J. Am. Chem. Soc.* **2005**, *127*, 7632–7637, DOI:10.1021/ja042192u.

(14) Nishijima, Y.; Ueno, K.; Yokota, Y.; Murakoshi, K.; Misawa, H. Plasmon-Assisted Photocurrent Generation from Visible to Near-Infrared Wavelength Using a Au-Nanorods/TiO2 Electrode. *J. Phys. Chem. Lett.* **2010**, *1*, 2031–2036, DOI:10.1021/jz1006675.

(15) Furube, A.; Du, L.; Hara, K.; Katoh, R.; Tachiya, M. Ultrafast Plasmon-Induced Electron Transfer from Gold Nanodots into TiO 2 Nanoparticles. *J. Am. Chem. Soc.* **2007**, *129*, 14852–14853, DOI:10.1021/ja076134v.
(16) Tang, Y.; Jiang, Z.; Xing, G.; Li, A.; Kanhere, P. D.; Zhang, Y.; Sum, T. C.; Li, S.; Chen, X.; Dong, Z.; Chen, Z. Efficient Ag@AgCl Cubic Cage Photocatalysts Profit from Ultrafast Plasmon-Induced Electron Transfer Processes. *Adv. Funct. Mat.* **2013**, *23*, 2932–2940, DOI:10.1002/adfm.201203379.
(17) Ratchford, D. C.; Dunkelberger, A. D.; Vurgaftman, I.; Owrutsky, J. C.; Pehrsson, P. E. Quantification of Efficient Plasmonic Hot-Electron Injection in Gold Nanoparticle–TiO2 Films. *Nano Lett.* **2017**, *17*, 6047–6055, DOI:10.1021/acs.nanolett.7b02366.
(18) Du, L.; Furube, A.; Yamamoto, K.; Hara, K.; Katoh, R.; Tachiya, M. Plasmon-Induced Charge Separation and Recombination Dynamics in Gold−TiO2 Nanoparticle Systems: Dependence on TiO2 Particle Size. *J. Phys. Chem. C* **2009**, *113*, 6454–6462, DOI:10.1021/jp810576s.
(19) Blandre, E.; Jalas, D.; Petrov, A. Yu.; Eich, M. Limit of Efficiency of Generation of Hot Electrons in Metals and Their Injection inside a Semiconductor Using a Semiclassical Approach. *ACS Photonics* **2018**, *5*, 3613–3620, DOI:10.1021/acsphotonics.8b00473.
(20) Neppl, S.; Gessner, O. Time-Resolved X-Ray Photoelectron Spectroscopy Techniques for the Study of Interfacial Charge Dynamics. *J. Electron Spectros. Relat. Phenom.* **2015**, *200*, 64–77, DOI:10.1016/j.elspec.2015.03.002.
(21) Seah, M. P.; Gilmore, I. S.; Beamson, G. XPS: Binding Energy Calibration of Electron Spectrometers 5—Re-Evaluation of the Reference Energies. *Surf. Interface Anal.* **1998**, *26*, 642–649.
(22) Erdem, B.; Hunsicker, R. A.; Simmons, G. W.; Sudol, E. D.; Dimonie, V. L.; El-Aasser, M. S. XPS and FTIR Surface Characterization of TiO2 Particles Used in Polymer Encapsulation. *Langmuir* **2001**, *17*, 2664–2669, DOI:10.1021/la0015213.
(23) Brack, M. The Physics of Simple Metal Clusters: Self-Consistent Jellium Model and Semiclassical Approaches. *Rev. Mod. Phys.* **1993**, *65*, 677–732, DOI:10.1103/RevModPhys.65.677.
(24) Bauer, D. Modeling the Core-Hole Screening in Jellium Clusters Using Density Functional Theory. *New J. Phys.* **2012**, *14*, 055012, DOI:10.1088/1367-2630/14/5/055012.
(25) Zapata Herrera, M.; Aizpurua, J.; Kazansky, A. K.; Borisov, A. G. Plasmon Response and Electron Dynamics in Charged Metallic Nanoparticles. *Langmuir* **2016**, *32*, 2829–2840, DOI:10.1021/acs.langmuir.6b00112.
(26) Smirnov, B. M. *Clusters and Small Particles: In Gases and Plasmas*; Springer Science & Business Media, 2012.
(27) Link, S.; El-Sayed, M. A. Spectral Properties and Relaxation Dynamics of Surface Plasmon Electronic Oscillations in Gold and Silver Nanodots and Nanorods. *J. Phys. Chem. B* **1999**, *103*, 8410–8426, DOI:10.1021/jp9917648.
(28) Nakade, S.; Saito, Y.; Kubo, W.; Kitamura, T.; Wada, Y.; Yanagida, S. Influence of TiO2 Nanoparticle Size on Electron Diffusion and Recombination in Dye-Sensitized TiO2 Solar Cells. *J. Phys. Chem. B* **2003**, *107*, 8607–8611, DOI:10.1021/jp034773w.
(29) Liang, L.; Dai, S.; Hu, L.; Kong, F.; Xu, W.; Wang, K. Porosity Effects on Electron Transport in TiO2 Films and Its Application to Dye-Sensitized Solar Cells. *J. Phys. Chem. B* **2006**, *110*, 12404–12409, DOI:10.1021/jp061284y.

(30) Benkö, G.; Kallioinen, J.; Korppi-Tommola, J. E. I.; Yartsev, A. P.; Sundström, V. Photoinduced Ultrafast Dye-to-Semiconductor Electron Injection from Nonthermalized and Thermalized Donor States. *J. Am. Chem. Soc.* **2002**, *124*, 489–493, DOI:10.1021/ja016561n.
(31) Němec, H.; Rochford, J.; Taratula, O.; Galoppini, E.; Kužel, P.; Polívka, T.; Yartsev, A.; Sundström, V. Influence of the Electron-Cation Interaction on Electron Mobility in Dye-Sensitized ZnO and TiO2 Nanocrystals: A Study Using Ultrafast Terahertz Spectroscopy. *Phys. Rev. Lett.* **2010**, *104*, 197401, DOI:10.1103/PhysRevLett.104.197401.